Journal of Catalysis **183,** 32–44 (1999)
Article ID jcat.1998.2386, available online at http://www.idealibrary.com on IDEAL®

Modifications in the Morphological and Chemical Properties of Copper Supported on Different Allotropic Forms of Carbon

J. Ma, N. M. Rodriguez, M. A. Vannice, and R. T. K. Baker

Department of Chemistry, Northeastern University, Boston, Massachusetts 02115; and Department of Chemical Engineering, The Pennsylvania State University, University Park, Pennsylvania 16802

Received June 23, 1998; revised November 30, 1998; accepted December 10, 1998

A combination of techniques including controlled atmosphere electron microscopy coupled with *in situ* electron diffraction has been used to follow the manner by which the nature of a carbonaceous support can impact both the chemistry and morphological properties of small copper particles when treated in various gas environments. We have found that the ease of reduction of CuO is dependent upon the nature of the carbon material and the strength of the interaction between the two components. It is suggested that an epitaxial relationship exists between copper and a diamond surface, which facilitates the reduction of copper oxide to the metallic state. In systems where copper species are supported on active carbon or graphite, attack on the substrate surface was observed to occur at low temperatures in the presence of hydrogen. This behavior is rationalized according to the notion that dissociation of molecular hydrogen takes place on Cu^0 sites at the surface of Cu_2O particles and that the active atomic species "spill over" onto the graphitic support media and undergo reaction with the π-electrons of the basal plane resulting in the creation of pits thus producing extensive modifications to the surface structure of these support media. Based on the data from *in situ* electron diffraction analysis it is tentatively concluded that at moderate temperatures under reducing conditions, Cu_2O is the stable chemical state on amorphous and graphitic forms of carbon.

INTRODUCTION

There are a number of commercial processes that utilize copper-containing catalysts for selective hydrogenation and methanol synthesis reactions (1, 2). Copper chromite catalysts have been traditionally used in industry for some of these reactions; however, the disposal of the spent catalyst now presents an environmental problem. As a consequence, there is an urgent need to replace such catalysts with less toxic materials, without sacrificing the high activity and selectivity afforded by the current system. Carbon supported copper particles appear to offer many of the benefits derived from copper chromite and therefore might provide an alternative, more acceptable catalyst system. Surface science studies of the chemical and physical properties of small copper particles supported on carbon surfaces have been carried out by various groups (3–6). Experiments performed on samples consisting of copper particles supported on graphite showed that when the particle size became very small, modified electronic properties were noted and these were associated with the variation of the *d*-band electron density. The *d*-band and the 2*p* core level peaks were found to move toward a higher bonding energy as the copper particle size decreased (3). The possible impact of these variations on the catalytic behavior of carbon supported copper particles has so far not been reported, but is currently being studied (7, 8).

The redox process of metallic copper and copper oxide is dependent on the reaction conditions, and different chemical states will certainly affect the catalytic activity. Jernigan and Somorjai (9) studied the catalytic behavior of different copper phases supported on graphite, namely metallic copper, Cu_2O, and CuO. They found that the stability of a given state of copper under CO oxidation conditions was a function of the oxidizing power of the CO/O_2 reactant ratio: metallic copper, Cu_2O, and CuO were stable at 97 : 3, 90 : 10, and 66 : 33 ratios, respectively. It should be emphasized, however, that there is considerable debate regarding the question of which particular copper species is the catalytically active entity.

In the current investigation we have endeavored to expand the study of carbon-supported copper by including an allotrope that has hitherto been neglected with regard to its potential as a catalyst support medium, namely diamond. Significant variations in the physical and chemical properties emerge among the different types carbonaceous materials. Activated carbon contains small domains of disordered graphitic structures and tends to have relatively poor electronic and thermal conductivity properties. On the other hand, graphite is the most stable phase of carbon and possesses both excellent electronic and thermal conductivity. Diamond is a metastable form of carbon and while it is an electrical insulator, it exhibits excellent thermal conducting properties (10).

While a considerable body of information exists relating to the bulk properties of diamond (11), it is surprising to

0021-9517/99 $30.00

find that, with the exception of some early studies using low-energy electron diffraction (LEED) (12, 13), comparatively little attention has been devoted to the investigation of the surface of the material until recent years (14–18). The role of chemisorbed hydrogen in promoting the reconstruction of certain crystallographic faces of diamond is an area of intense research activity (14, 16, 19–21). It is generally believed that the diamond (111) surface contains adsorbed hydrogen (15) and that reconstruction of the face occurs upon heating to 1000°C, at which stage the hydrogen is desorbed and the appearance of surface states is observed (22). It is found experimentally that the reconstructed surface selectively adsorbs atomic rather then molecular hydrogen, and under these conditions the surface states disappear and the electronic structure relaxes back to that of the 1×1 bulk surface (14, 22).

Baker and co-workers (23, 24) used controlled atmosphere electron microscopy to study the dynamic behavior of copper particles supported on graphite and magnesium oxide as these specimens were heated in the presence of various gaseous environments. Copper was found to be an extremely active catalyst for the graphite–oxygen reaction over the range 550 to 800°C and under these conditions it was postulated that CuO was the active entity. Continuous observation of the reaction showed that at 520°C the metal oxide particles located at the graphite edge regions underwent a transformation from a nonwetting to a wetting state. This change in morphology was accompanied by the onset of catalytic oxidation of carbon seen as the creation of channels across the substrate basal plane surfaces. As the temperature was progressively raised the wetting action of the particles on graphite intensified and material was deposited on the sides of the channels as a result of a spreading action. This behavior resulted in a change in the mode of catalytic attack from channeling to edge recession. The results of this study highlighted the fact that not only the interaction between metal and support exerts an influence on the morphology of the metal particles, but the nature of the reactant gas can also play a critical role in modifying the surface arrangement of atoms in a solid and, as a consequence, be responsible for inducing changes in the structure of small particles (23).

This aspect was further substantiated in a similar type of investigation where Cu–MgO specimens were initially heated in oxygen and then in hydrogen (24). When the system was heated in oxygen at 200°C, the metal particles were observed to undergo an extraordinary transformation, with discrete solid crystallites changing to toroidal shaped oxide structures. Subsequent treatment in hydrogen at 200°C resulted in the restoration of the original metallic globular form. These results were discussed in terms of a volcano structure, in which particles consisted of a molten metal core surrounded by a porous solid oxide skin.

Other workers (25) have used transmission electron microscopy (TEM) to determine the average particle sizes of copper crystallites dispersed on magnesium oxide; however, no mention was made in these studies of their morphological characteristics. Pilliar and Nutting (26) used a novel specimen arrangement that enabled them to observe the profiles of copper particles supported on α-alumina at high magnifications. From these studies an attempt was made to derive the interfacial energy parameters of the supported metal particles. These experiments were performed under post-reaction conditions where the specimens had been cooled to room temperature and during transfer to the electron microscope were exposed to air and as such, the morphological characteristics of the metal particles may not have been representative of the appearance during reaction.

An earlier paper from our group focused on the characterization of copper chromite catalysts using the hydrogenation of furfural and crotonaldehyde as probe reactions of the system (27). These studies were complemented by hydrogen and carbon monoxide chemisorption and *in situ* DRIFTS. From these experiments it was concluded that Cu^+ sites were involved in the reactions, but the participation of Cu^0 species was also invoked. A survey of the catalysis literature has revealed the existence of a very limited amount of information regarding the use of the copper–carbon system. The results of some studies have been reported on the use of copper oxide dispersed on activated carbon (28, 29), activated carbon fibers (30), and coal (31) as catalysts for NO conversion reactions. In these cases, however, no efforts were made to examine either the particle size distributions or the morphological characteristics of the copper crystallites. In the current investigation, we have used a combination of controlled atmosphere electron microscopy, high resolution transmission electron microscopy, and *in situ* electron diffraction techniques to examine the behavior of copper particles supported on different types of carbon materials when heated in oxygen and hydrogen environments. These experiments have enabled us to gain a clearer understanding of some of the complexities of the copper–carbon system.

EXPERIMENTAL

Materials

The origin, shorthand designations, and some of the characteristics of the allotropic forms of carbon that were used as the support media in this study are given in Table 1. Prior to impregnation with copper salts all support materials were treated in 1 *M* nitric acid for periods of 5 days in order to remove any extraneous inclusions. The various carbon-supported samples were prepared from a $Cu(NO_3)_2$ precursor salt using a wet impregnation method to achieve

TABLE 1

Origin and Characteristics of the Carbonaceous Substrates

Substrate	Notation	Supplier	N_2 surface area (m^2/g)
Active carbon	AC	American Norit Co.	800
Pitch fiber	PF	Amoco Performance Products	6
Diamond powder	D	Alpha Chemical Co.	8
SP1 graphite	G	Union Carbide	1

a 5% copper loading. The impregnated samples were dried overnight in air at 110°C, calcined in air at 150°C for 12 h, purged with helium, and then reduced in a 10% H_2–He mixture at 300°C for 24 h. After reduction, all the samples were cooled to room temperature in He and subjected to a passivation process where a 2% O_2–He mixture was allowed to flow over the catalysts at room temperature for 1 h before removal from the reactor. The copper salts were purchased from Fisher Scientific and the gases used in these experiments, hydrogen (99.999%), oxygen (99.99%), and helium (99.99%), were obtained from MG Industries and used without further purification.

Techniques and Procedures

Controlled atmosphere electron microscopy studies were carried out in the modified JEOL 2000 EXII instrument that is equipped with a custom-designed environmental cell, which accommodates a Gatan heating stage. With this technique it is possible to directly observe the changes in appearance of a specimen as it is heated from room temperature up to 1000°C in the presence of 1 to 5 Torr of a reactant gas. The dynamics of the reaction taking place at the specimen surface were displayed on a TV monitor and continuously recorded on video tape. The point to point resolution achieved on the TV monitor was estimated to be better than 0.4 nm. A detailed description of this technique and procedures used to perform *in situ* studies can be found elsewhere (32). When operated in the electron diffraction mode, detailed information on the chemical state of the specimen can be obtained at any stage of the reaction. Transmission specimens of single crystal graphite were prepared by a standard cleaving procedure and diamond powder dispersed on holey carbon grid was used as the support media in the electron microscopy studies. Copper was introduced onto these samples by the atomized spray of 0.1 wt.% aqueous solution of $Cu(NO_3)_2$. For the *in situ* electron diffraction experiments, a somewhat heavier metal precursor loading, to give about four monolayer metal thickness, was introduced onto the carbon substrates. Electron diffraction patterns were taken at various stages of the reaction as the specimens were heated in 0.5 Torr hydrogen. Analysis of the patterns was performed by measuring the vector of the graphite primary diffraction spots ($d_{100} = 2.131$) and the radii of the diffraction rings on the photographic negatives to an accuracy of 0.05 mm. The graphite primary diffraction spots were used as the internal standard to correct for variations in camera length. The measured diffraction radii were then used to calculate the *d*-spacing of the crystallographic plane responsible for creating the rings and then compared with *d*-spacing values of possible reaction products as obtained from the standard crystallographic data (33).

In another series of experiments the electron microscope was utilized in its conventional high resolution mode to determine the particle size distributions of passivated supported copper specimens that were treated in a horizontal flow reactor system in the presence of a series of gases. For these examinations samples of the various catalysts were dispersed in iso-butanol and a drop of the supernate introduced onto a holey carbon substrate. In each case particle size distributions were obtained from measurements of over 400 particles located in different regions.

Bulk determinations of the copper crystalline phases present after preparation were identified by X-ray diffraction (XRD) on a Scintag XDS-2000 diffractometer using Cu $K\alpha$ (45 kV, 40 mA) radiation. Temperature programmed reduction (TPR) studies of copper oxide on the different carbonaceous supports was performed on a custom-designed unit equipped with a thermal conductivity detector. In these experiments a 10% H_2–N_2 gas mixture was used as both the reduction and the carrier gas for the detector. The sample was heated at the rate of 10°C/min in the gas mixture with a total flow rate of 50 mL/min. A cold trap was inserted in the line to remove the water generated in the reaction. In a further series of experiments a thermogravimetric technique was used to perform temperature programmed oxidation and isothermal reduction studies of carbon-supported copper catalyst samples. These experiments were carried out with a Cahn 2000 vacuum microbalance system. Output signals were collected and stored by an online computer. BET surface area of the catalysts were measured by N_2 physisorption at −196°C using an Omnisorb 100CX automatic gas sorption analyzer.

RESULTS

Catalyst Preparation

The preparation conditions of copper–carbon catalysts were directly associated with the nature of the carbonaceous supports and the redox properties of copper species. The chemical state of copper species on these supports was determined via post-reaction analysis by XRD. As shown in Table 2, reduction of cupric oxide to the metallic state was most difficult to achieve when supported on activated carbon, while this transformation was easily accomplished with a diamond carrier. Cuprous oxide, Cu_2O, was found to be present in the copper–activated carbon catalyst system even after a 72 h reduction period, and under the

TABLE 2

Chemical State of Reduced Copper–Carbon Catalysts

	Possible chemical state		
	Reduction time (h)		
Catalyst	24	48	72
Cu/AC	Cu^0, **Cu^{+1}**	Cu^0, **Cu^{+1}**	Cu^0, **Cu^{+1}**
Cu/GF	Cu^0, **Cu^{+1}**	Cu^0, Cu^{+1}	Cu^0
Cu/D	Cu^0	Cu^0	Cu^0

Note. The copper loading is 5 wt%. The reduction temperature is 300°C. Data shown in boldface denote the dominant phase.

same conditions it was also present in the copper–carbon fiber system after 24 h. These findings indicate that the ease of reduction of copper oxide to the metallic state exhibits a significant variation as a function of the type of carbonaceous material utilized as the support medium.

Temperature Programmed Reduction

Temperature programmed reduction provides a complementary method to probe the extent of the reduction process of carbon-supported copper catalysts. The reduction of pure cupric oxide exhibited a single sharp asymmetric peak at about 280°C, with an unidentified shoulder on the low temperature side, representing the facile conversion of the chemical state of copper species from +2 to 0. Similar patterns have been reported by other workers for the reduction of CuO (34, 35) and consistent with the present data, no evidence was obtained to indicate the transient existence of Cu^+ species during this treatment. When this procedure was conducted on samples where CuO particles were supported on carbonaceous materials it was evident that the reduction process occurred in a step-wise fashion. This aspect can be seen from inspection of the TPR patterns of cupric oxide and carbon-supported cupric oxide particles presented in Fig. 1, where the appearance of two oxide reduction peaks occurs with all the supported systems. It is also apparent that the onset of the reduction of cupric oxide on diamond is observed at the lowest temperature. In these experiments we are only detecting the difference of the hydrogen concentration in the feed gas before and after the reactor. Under such circumstances the small consumption of hydrogen due to the formation of hydrocarbons from surface pitting reactions giving rise to hydrogasification of the carbonaceous supports would probably not be apparent in the signal.

It should be appreciated that the reduction of supported metal oxides is not a simple task and a so-called slow reduction process merely implies that a significant amount of Cu^+ species exist at any given point in time, confirming that this is an intermediate state in the reaction. If this reaction was conducted on a support such as γ-alumina the complete reduction step would require several days to accomplish and as a consequence the relative peak sizes of the two oxide states would exhibit a continuous change over this period. One might expect that differences in the metal oxide particle size would play a role in the rate of the reduction process. In the current work, however, the average particle sizes on all the carbonaceous supports were quite similar and so such an effect is unlikely to be operative. Instead, it is more probable that the observed variations in behavioral patterns are due to differences in the strength of the interactions between the oxide particles and the supports.

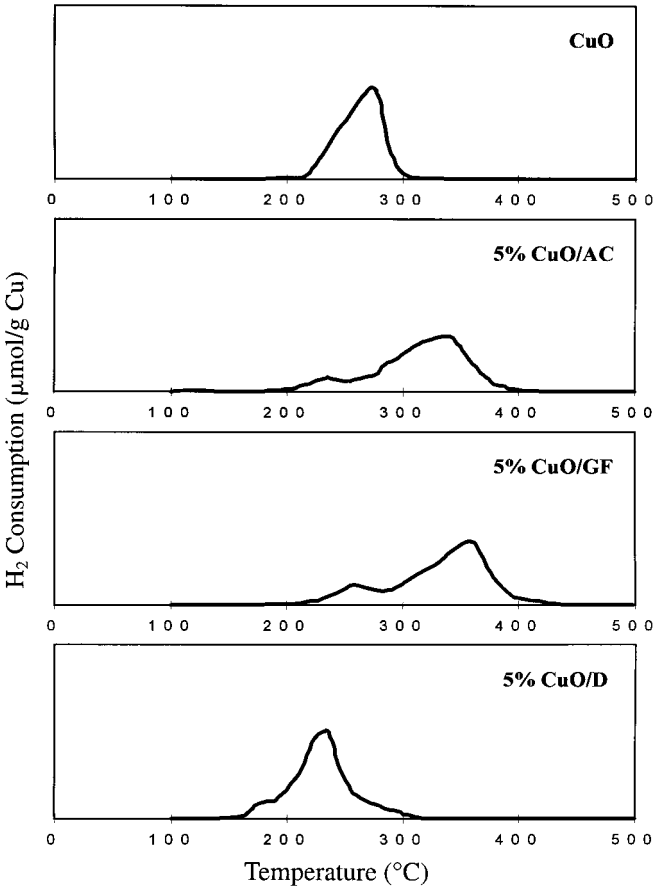

FIG. 1. Temperature programmed reduction patterns of CuO, 5% CuO–active carbon, 5% CuO–graphitic fibers, and 5% CuO–diamond.

BET Surface Area Measurements

The N_2 BET surface areas of the various types of carbon used in this investigation along with changes that occurred when copper was dispersed on the respective materials are given in Table 3. It can be seen that the active carbon sample exhibits a surface area that is about two orders of magnitude higher than that of either the graphitic carbon fibers or diamond powder. The introduction of copper onto the diamond and carbon fiber substrates and subsequent reduction procedure exerted only a marginal influence on the overall surface area of these systems although both increased.

TABLE 3

Surface Area of Reduced Copper–Carbon Catalysts

	Surface area (m^2/g)			
	Reduction time (h)			
Catalyst	0	24	48	72
Cu/AC	800	807	1037	1224
Cu/GF	6	9	16	15
Cu/D	8	12	11	13

Note. The copper loading is 5 wt%. The reduction temperature is 300°C.

In contrast, when the copper–active carbon samples were given the same treatments a significant increase in the surface area was observed.

TEM Examinations

Transmission electron microscopy is routinely used to determine the particle size distribution of supported metal catalysts. More recently, it has been recognized that the technique can yield much more fundamental information, particularly with regard to the location and morphological characteristics of metal particles, and this information can provide an insight into the nature of the interaction with the support medium. In addition, when the microscope is operated in the diffraction mode, it is a relatively simple task to determine the chemical state and the probable orientation of the metal particles.

Examination of the three types of carbon-supported copper samples revealed the existence of two distinct particle morphologies following heat treatment of the systems in H_2. Following reduction at 100°C, copper particles supported on either activated carbon or graphite fibers were found to adopt a toroidal (or "donut") geometry. It was interesting to find that this condition was not achieved when copper–diamond samples were subjected to the same treatment. In this case, the particles acquired a solid hexagonal-shaped form, a morphological arrangement that was also predominant in the other two carbon-supported copper systems when the reduction temperature was raised to 300°C.

The copper particle size distributions on the three types of carbonaceous supports following treatment in hydrogen at 300°C for periods of 24 and 72 h, respectively, are presented in Figs. 2–4. These measurements, which were taken from several regions of a given specimen, enabled one to estimate average sizes of copper particles on activated carbon, graphite fibers, and diamond to be 14.5, 12.2, and 15.6 nm, respectively, after the 24 h reduction time. In experiments where the reaction was allowed to proceed for a longer period, it is evident that metal sintering took place on both the activated and fibrous carbon supports, whereas the copper particle size distribution remained relatively stable on the diamond support.

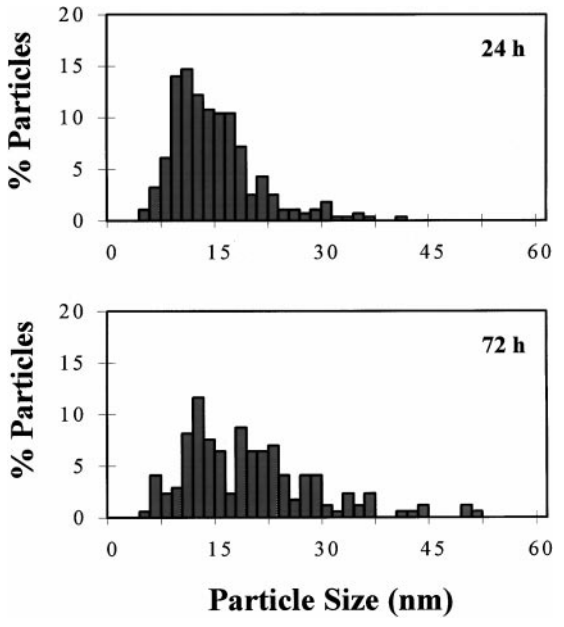

FIG. 2. Particle size distribution of 5% Cu–active carbon after treatment in hydrogen at 300°C for periods of 24 and 72 h.

Controlled Atmosphere Electron Microscopy (CAEM) Experiments

Copper–graphite–hydrogen. Examination showed that the initial CuO–graphite specimen, which had been generated from the calcination of cupric nitrate in air at 300°C, was in the form of a thin film spread across the substrate surface. This sample was subsequently heated in 1 Torr

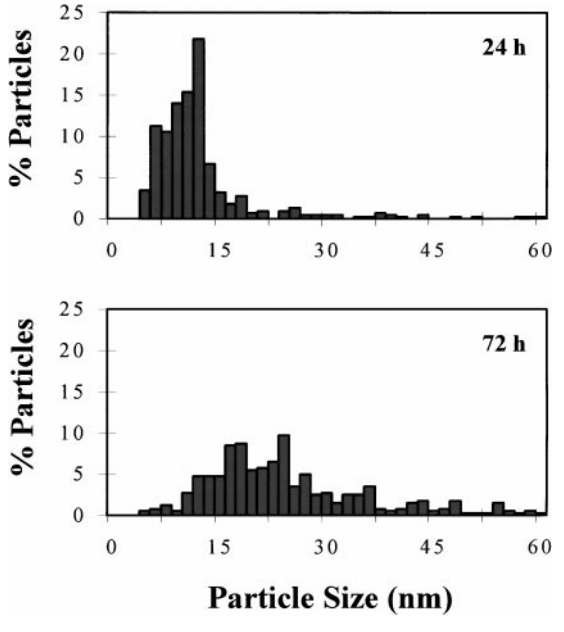

FIG. 3. Particle size distribution of 5% Cu–graphitic fibers after treatment in hydrogen at 300°C for periods of 24 and 72 h.

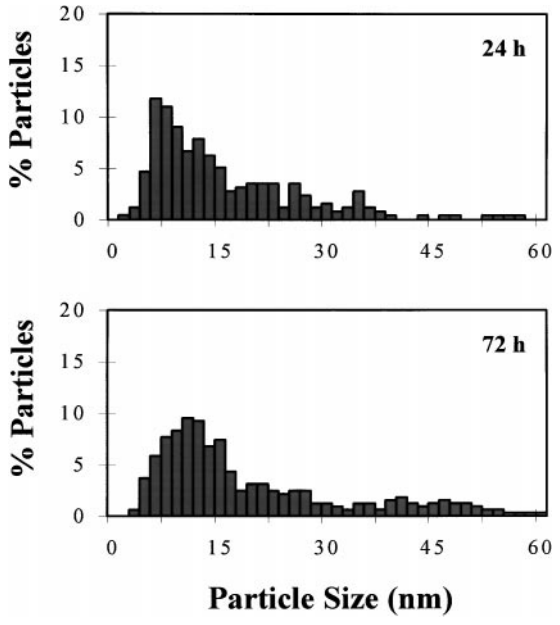

FIG. 4. Particle size distribution of 5% Cu–diamond after treatment in hydrogen at 300°C for periods of 24 and 72 h.

hydrogen within the electron microscope. Continuous observation of this process showed that when the temperature was gradually raised to 75°C, the oxide film started to undergo nucleation and collected into small islands. During this stage of the reaction, pits were observed to form on the basal plane of the graphite and to proceed to expand and become progressively deeper, a condition that can be seen in the electron micrograph, Fig. 5. The boundaries of the pits appeared to be highlighted because of the accumulation of copper species at these sites. Determinations of the rate of the pit edge recession were derived from the measurements of the recorded sequences showing the linear increase in size as a function of time. Examples of two such pit expansion plots are presented in Fig. 6, from which it has been possible to estimate values of 0.83 to 0.91 nm/s for the rate of edge recession at 100°C.

At the same time, it was evident that other copper species were forming into toroidal (donut) shaped particles and a survey of many different specimen areas indicated that this behavior was widespread at 100°C. An example of these structures is shown in the electron micrograph, Fig. 7, which was taken during the reaction. Examination of a specimen from a complementary experiment performed in a flow reactor at atmospheric pressure at 50°C for 1 h in the presence of a 10% H_2–He showed the existence of the same pattern

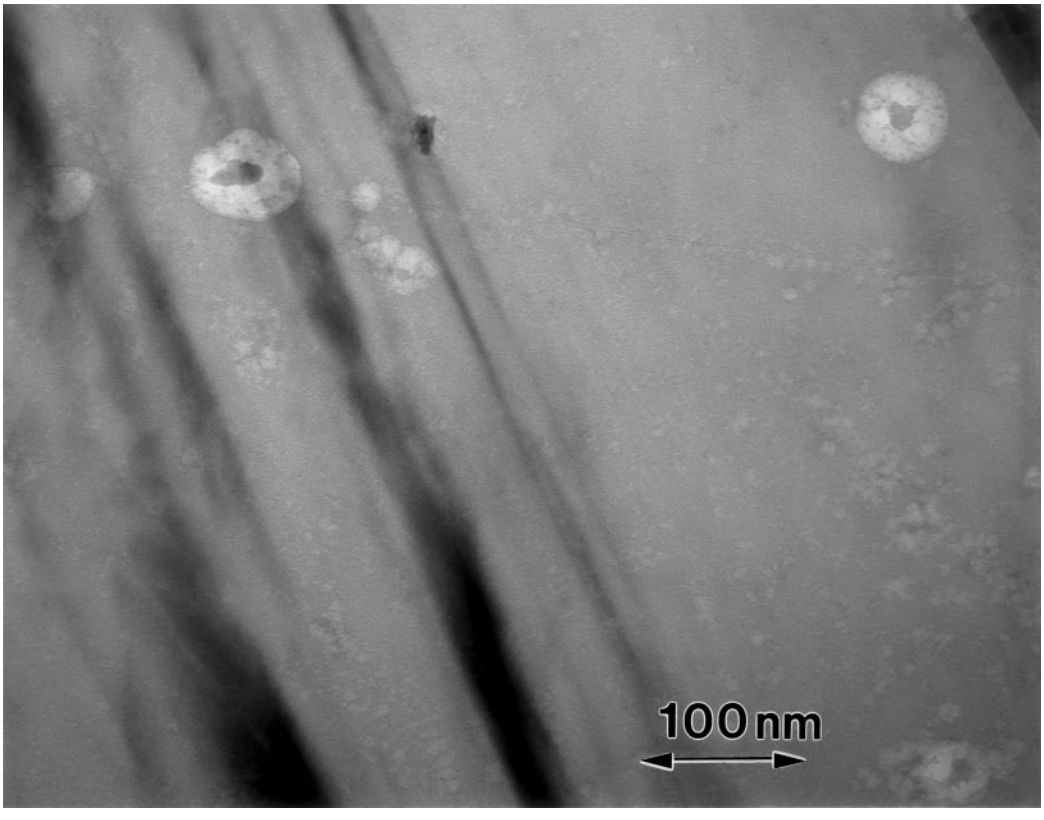

FIG. 5. Transmission electron micrograph of a copper–graphite specimen taken during reaction in 1.0 Torr hydrogen at 100°C showing the formation of pits in the basal plane surface of the substrate.

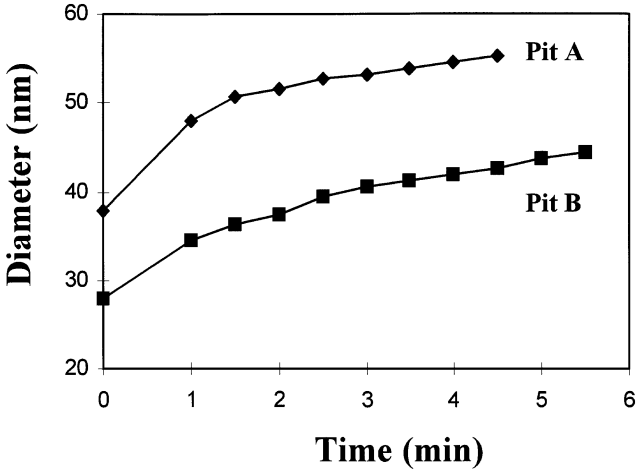

FIG. 6. Expansion in the width of two different initial-sized pits formed in the surface of a copper–graphite specimen during heating in 1.0 Torr hydrogen over a period of 6 min at 100°C.

of behavior, suggesting that this sequence of events was not limited to the low-pressure condition encountered in the environmental cell of the electron microscope and, furthermore, was not an artifact resulting from irradiation effects of the electron beam. In addition, the creation of pits in the graphite basal plane regions was a general phenomenon since these features were found to form over the entire surface of the specimen. The possibility that irradiation effects were operative was checked by performing a blank experiment where the electron beam was switched off during the heating period of 1.0 h at 100°C, and the sample was examined only after cooling to room temperature. The appearance of the graphite surface was identical to that where continuous observation of the reaction had been conducted.

As the temperature was gradually increased to 300°C, the toroidal structures were observed to undergo a dramatic change in geometrical form. In some cases the ring-like structures ruptured to generate numerous smaller solid particles or, alternatively a collapse of the toroids occurred with subsequent rearrangement to form well-defined hexagonal shaped particles. The typical appearance of a specimen at this stage of the reaction is presented in Fig. 8. It was significant to find that the attack of the graphite basal plane no longer proceeded at this higher temperature. A schematic representation of the sequence of events and changes in particle morphology is given in Fig. 9. In this diagram CuO particles undergo a change in morphology from thin flat pillbox to toroidal structures at 100°C. Examination of the latter structures by TEM only provides a 2-D image and therefore we cannot be sure of the topographical features

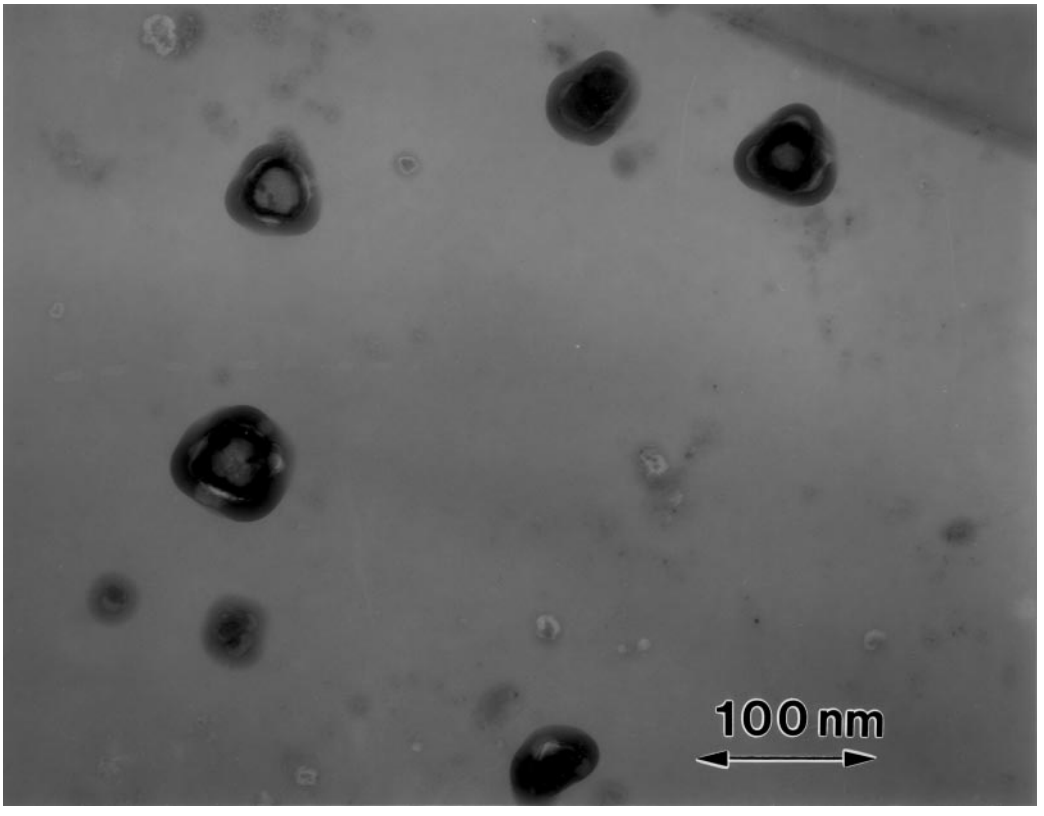

FIG. 7. Transmission electron micrograph showing the formation of a toroidal shaped copper particles on graphite during reaction in 1.0 Torr hydrogen at 100°C.

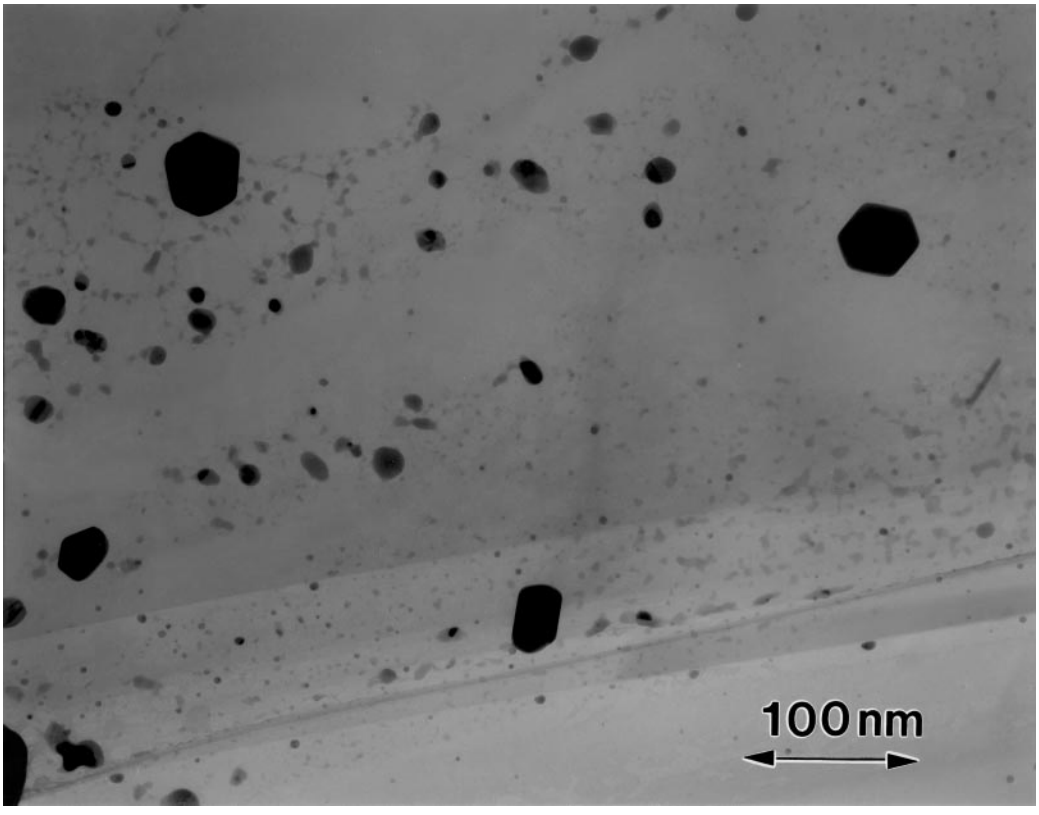

FIG. 8. Transmission electron micrograph showing the appearance of well-defined hexagonal shaped copper particles on graphite formed in the presence of 1.0 Torr hydrogen at 300°C.

of such entities. According to the transmission image such particles consist of an electron dense ring surrounding a less dense core, but it is not possible to ascertain if these two regions are in different chemical states. This transformation is accompanied by the creation of shallow pits in the graphite basal plane regions immediately adjacent to the metal oxide particles. On, continued heating to 300°C, the particles undergo a further change in morphology to form thin hexagonal structures and at the same time catalytic attack of the graphite substrate ceases. The whole process

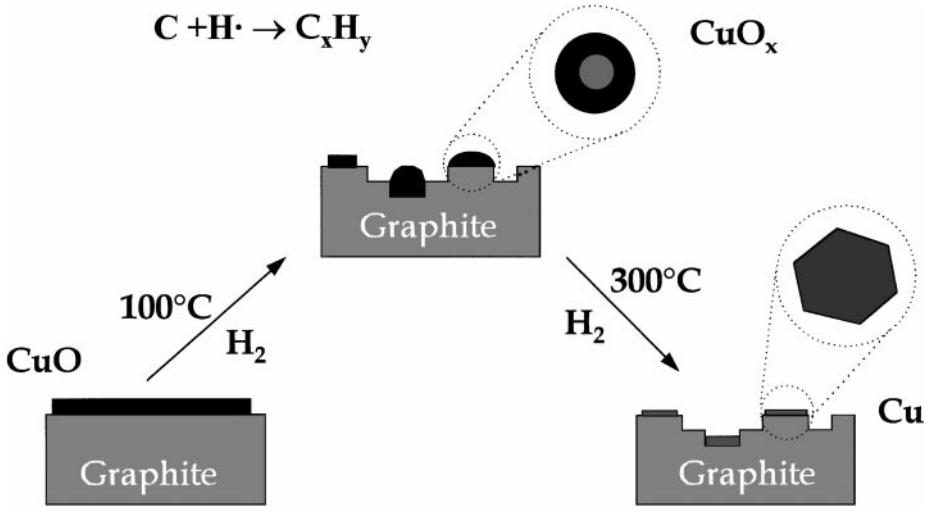

FIG. 9. Schematic rendition of the changes in copper particle morphology resulting from treatment in 1.0 Torr hydrogen as the temperature was progressively raised from 50 to 300°C.

could be reversed by an oxygen treatment of the reduced specimen before repeating the reaction with hydrogen. In some experiments the reaction in hydrogen was extended to 800°C and under these circumstances copper particles that were located at graphite edges were observed to undergo a wetting action in these regions and subsequently proceed to catalyze the formation of channels across the basal planes.

Copper–graphite–oxygen. When prereduced copper–graphite specimens were heated in the presence of 1 Torr oxygen at 300°C, particles that had collected at the edge regions of the support were observed to decrease gradually in size as they underwent a wetting and spreading action along the graphite surface. This behavior is associated with the establishment of a strong interaction between the metal oxide particles and oxygenated graphite edge atoms. It was interesting to find that change in particle morphology was not accompanied by the removal of carbon at this temperature. When the temperature was increased to 450°C, the contaminated graphite edge regions were observed to undergo gasification via the edge recession mode. The rudiments of this form of catalyzed attack of graphite has been covered in a detailed fashion previously (36).

Copper–diamond–hydrogen. When the preoxidized samples were initially examined at room temperature, it was not possible to discern the presence of any particles on the diamond surface, thus suggesting that copper species were in the form of a thin film spread over the surface. This condition was found to persist when the system was subsequently treated in 1.0 Torr hydrogen up to 100°C. In contrast to the copper–graphite behavior, however, no sign of any type of pitting attack of the diamond surface was observed at this temperature. When the temperature was increased to 300°C, the copper film broke up to form islands, which eventually nucleated into discrete hexagonal-shaped particles. Close inspection of these structures showed that the metal crystallites that collected on the edges were relatively large whereas those formed on the diamond basal plane tended to be much smaller on average and possessed a thin, flat morphology, as shown in Fig. 10. It was noticeable that in this system no evidence of the particles adopting an intermediate toroidal geometry was observed during the temperature excursion from 100 to 300°C. In experiments where the temperature was raised to a maximum of 700°C, it was interesting to find that not only was there a complete absence of catalytic attack of the support medium, but also that particle sintering was quite limited even though the set temperature was appreciably higher than that of the Tammann temperature of copper, 405°C, which is calculated from 0.52 bulk melting point (K).

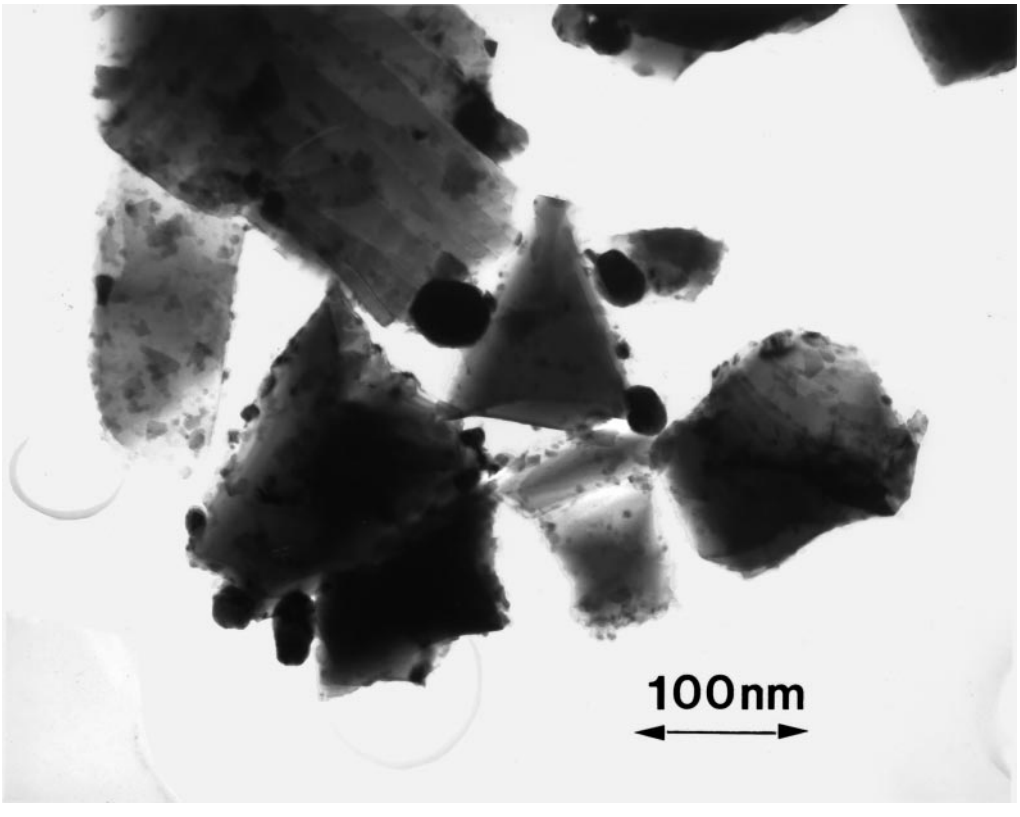

FIG. 10. Transmission electron micrograph of a copper/diamond specimen undergoing reaction in 1.0 Torr hydrogen at 300°C.

In Situ Electron Diffraction Analysis

In order to determine the chemical state of the copper species present at various stages during the reduction process, *in situ* electron diffraction patterns were taken at selected temperatures during the treatment of copper–graphite and copper–diamond specimens in 0.5 Torr hydrogen. Both of these samples had been previously calcined in air at 300°C for 5 h before being transferred to the electron microscope. Diffraction patterns were taken at selected temperatures as the specimens were gradually heated to 450°C. This operation was only carried out after the respective sample had been held at a given temperature for a period of 15 min. The sets of experimentally determined *d*-spacings of various diffracting species for both systems, as calculated from the electron diffraction data are presented in Tables 4 and 5.

Inspection of these data shows some very interesting features and demonstrates the existence of some major differences in the chemistry of these two systems as the temperature is progressively increased. It is apparent that in both systems CuO is the dominant bulk species at 100°C. The formation of tangible amounts of Cu_2O species are detected on the diamond substrate at 200°C and on the graphite support at 300°C. Upon continued heating to higher temperatures it is evident that Cu_2O becomes the primary state on graphite at 400°C and that temperatures in excess of 450°C are required to achieve complete reduction to the metallic state. In contrast, when the particles are dispersed on the diamond carrier, stabilization of the Cu_2O phase is more difficult to realize because conversion to the metallic state occurs quite readily at 300°C. A further aspect that is encountered in this system is that the *d*-spacing of the $Cu_{(111)}$ and $diamond_{(111)}$ faces are very close and as a consequence one cannot determine with any degree of certainty which particular faces are in contact at the metal–support interface.

TABLE 4

Electron Diffraction Pattern Analysis of Graphite Supported CuO as a Function of Temperature in 0.5 Torr H_2

Temperature (°C)	Calculated *d*-spacings (Å)	*d*-spacing (Å)			
		Cu	Cu_2O	CuO	Graphite
100	2.757			**2.752**$_{(110)}$	
	2.523		2.465$_{(111)}$	**2.524**$_{(111)}$	
	2.341			**2.311**$_{(200)}$	
	1.952			**1.961**$_{(112)}$	1.958$_{(012)}$
	1.854			**1.867**$_{(202)}$	
	1.582			**1.581**$_{(202)}$	
	1.499			1.506$_{(113)}$	
	1.407			1.409$_{(311)}$	
	1.384			1.375$_{(220)}$	
	1.301			1.304$_{(311)}$	
	1.269			1.266$_{(004)}$	
	1.162			1.170$_{(313)}$	1.153$_{(113)}$
	1.011				
	0.979		**0.980**$_{(331)}$		0.990$_{(116)}$
	0.880		**0.872**$_{(422)}$		
300	2.549			2.531$_{(002)}$	
	1.953			**1.961**$_{(112)}$	1.958$_{(012)}$
	1.877			**1.867**$_{(202)}$	
	1.723		**1.743**$_{(211)}$	**1.712**$_{(020)}$	
	1.592			**1.581**$_{(202)}$	
	1.503		**1.510**$_{(220)}$	1.506$_{(113)}$	
	1.407			1.409$_{(311)}$	
	1.395			**1.379**$_{(113)}$	
	1.308		1.287$_{(311)}$	1.304$_{(311)}$	
	1.265	1.278$_{(220)}$		1.262$_{(222)}$	
	1.167			1.170$_{(313)}$	1.153$_{(113)}$
	1.013				
	0.977		**0.980**$_{(331)}$		0.990$_{(116)}$
	0.936		0.955$_{(420)}$		
	0.929				
	0.882		**0.872**$_{(422)}$		
400	3.031		3.020$_{(110)}$		
	2.517			**2.524**$_{(111)}$	
	2.445		**2.465**$_{(111)}$		
	1.743		**1.743**$_{(211)}$		
	1.502		**1.510**$_{(220)}$	1.506$_{(113)}$	
	1.278	**1.278**$_{(220)}$	1.287$_{(311)}$		
	1.220		**1.233**$_{(222)}$		1.228$_{(110)}$
	1.066		**1.067**$_{(400)}$		1.081$_{(018)}$
	0.973		**0.980**$_{(331)}$		0.990$_{(116)}$
	0.948		0.955$_{(420)}$		
	0.869		**0.872**$_{(422)}$		
450	3.075		**3.020**$_{(110)}$		
	2.511		2.465$_{(111)}$	2.524$_{(111)}$	
	1.860			1.867$_{(202)}$	
	1.522		**1.520**$_{(220)}$	1.506$_{(113)}$	
	1.291	**1.278**$_{(220)}$	**1.287**$_{(311)}$	1.304$_{(311)}$	
	1.102	**1.090**$_{(311)}$		1.091$_{(131)}$	1.116$_{(009)}$
	1.050	**1.044**$_{(222)}$	**1.067**$_{(400)}$		
	0.837	**0.829**$_{(331)}$	0.822$_{(511)}$		0.837$_{(012)}$

Note. Data shown in boldface denote dominant phase.

DISCUSSION

The most significant aspect to emerge from this investigation is the finding that when different allotropic forms of carbon are used to support copper, major perturbations in both the chemical state and particle morphology can be observed as a function of the reduction conditions in hydrogen. In addition, it has been found that the dissociation of hydrogen on cuprous oxide particles (Cu_2O) at temperatures as low as 100°C can generate species that are capable of attacking the basal plane regions of a graphitic substrate. Based on a DRIFTS study of CO adsorbed on these catalysts at −100°C, it is very likely that the dissociation occurs on Cu^0 sites that exist at the surface of these oxide particles (7). Both macro and micro experiments indicated that this phenomenon led to an increase of the surface area of graphite surface during the reduction process. For the sake

TABLE 5

Electron Diffraction Pattern Analysis of Diamond Supported CuO as a Function of Temperature in 0.5 Torr H_2

Temperature (°C)	Calculated *d*-spacings (Å)	*d*-spacing (Å)			
		Cu	Cu_2O	CuO	Diamond
100	2.758			**2.752**$_{(110)}$	
	2.513		2.465$_{(111)}$	**2.524**$_{(111)}$	
	2.294			**2.311**$_{(200)}$	
	2.060	2.088$_{(111)}$			2.06$_{(111)}$
	1.706			**1.712**$_{(020)}$	
	1.403			**1.409**$_{(311)}$	
	1.254	1.278$_{(220)}$	1.233$_{(222)}$	**1.262**$_{(222)}$	1.261$_{(220)}$
	1.070	1.090$_{(311)}$	1.067$_{(400)}$		1.075$_{(311)}$
200	2.532		**2.465**$_{(111)}$	**2.524**$_{(111)}$	
	2.328			**2.311**$_{(200)}$	
	2.059	2.088$_{(111)}$			2.06$_{(111)}$
	1.489	1.278$_{(220)}$		**1.506**$_{(113)}$	
	1.406	1.090$_{(311)}$		**1.409**$_{(311)}$	
	1.255		**1.233**$_{(222)}$	**1.262**$_{(222)}$	1.261$_{(220)}$
	1.070		**1.067**$_{(400)}$		1.075$_{(311)}$
300	2.775			2.752$_{(110)}$	
	2.528		**2.465**$_{(111)}$	2.524$_{(111)}$	
	2.336			2.311$_{(200)}$	
	2.060	**2.088**$_{(111)}$			2.06$_{(111)}$
	1.722		**1.743**$_{(211)}$	1.712$_{(020)}$	
	1.641				
	1.515		**1.510**$_{(220)}$	1.506$_{(113)}$	
	1.441				
	1.265	**1.278**$_{(220)}$	**1.287**$_{(311)}$	1.262$_{(222)}$	1.261$_{(220)}$
	1.082	**1.090**$_{(311)}$	**1.067**$_{(400)}$	1.091$_{(131)}$	1.075$_{(311)}$
	1.025	**1.044**$_{(222)}$			
	0.819	**0.829**$_{(331)}$	**0.822**$_{(511)}$		0.818$_{(331)}$
400	2.060	**2.088**$_{(111)}$			2.06$_{(111)}$
	1.234	**1.278**$_{(220)}$	1.287$_{(311)}$		1.261$_{(220)}$
	1.178			1.170$_{(313)}$	
	1.058	**1.044**$_{(222)}$	1.067$_{(400)}$		1.075$_{(311)}$
	0.910	**0.904**$_{(400)}$			
	0.796	**0.808**$_{(420)}$			0.818$_{(331)}$

Note. Data shown in boldface denote dominant phase.

of simplicity these features will be dealt with separately in the proceeding discussion.

(a) Impact of Support on Copper Particle Morphology

Direct observation of the behavior of copper particles on graphite and diamond showed that in the fully oxidized state copper undergoes a wetting and spreading action on the basal surfaces of both of these materials, which is indicative of the establishment of a strong interaction between the metal oxide and the support medium. When these systems were subsequently heated in hydrogen, the resultant behavior was extremely sensitive to the type of carbon used as the carrier. Treatment in hydrogen of CuO–graphite specimens showed a behavior similar to that observed from post-reaction examinations of bulk samples where the metal oxide was dispersed on either graphitic fibers or activated carbon supports.

At temperatures of about 100°C, nucleation of the metal oxide film into discrete particles was observed to proceed via the formation of toroidal-shaped structures. The existence of these unusual particle geometries has been reported previously (37–41), and the thermodynamic perspectives of the formation of such structures has been discussed in a very comprehensive manner by Ruckenstein (42). Before proceeding into a detailed discussion of possible growth mechanisms, one must be aware that since conventional transmission electron microscopy only provides a 2-D image of these particles, the possibility that they could in reality be hollow spheres should not be overlooked, a contention made by Chen and co-workers (40). Indeed, this feature has been highlighted in some very sophisticated electron microscopy studies performed by Datye and coworkers (43) who used holographic techniques to demonstrate that such a particle geometry could exist, particularly under conditions where an oxide was undergoing transition to metal and vice versa.

Upon continued heating to higher temperatures, electron diffraction data indicated that most of the cupric oxide was reduced to the metallic state, a transformation that took place more readily on diamond than on the other allotropic forms of carbon. This feature was also observed using subambient CO adsorption techniques (7). With both graphite and diamond substrates, when complete reduction of the copper species had been achieved, the particles were found to acquire similar morphological characteristics: a relatively flat, hexagonal-shaped form. Furthermore, it was frequently possible to discern textural features of the support through the particles, indicating that such crystallites were very thin. It is suggested that the elimination of adsorbed oxygen groups from the graphite and diamond surfaces, in concert with the conversion of CuO to Cu creates the conditions required for the establishment of a strong metal–support interaction, which is reflected in the crystallite morphology.

(b) Effect of the Copper Oxide–Hydrogen Reaction on the Surface Structure of the Support

The finding that active species generated from the interaction between copper oxide and hydrogen were found to be capable of creating pits in the basal plane regions of graphite at very low temperatures (<100°C) is quite fascinating. Previous studies of the copper–graphite–hydrogen system revealed that catalytic gasification of the substrate by metal particles was only observed at temperatures in excess of 800°C, and furthermore, the attack occurred exclusively by the channeling mode (23). Therefore, it is evident that in order to account for the low-temperature pitting action described above, an alternative mechanism must be

operative. The CAEM experiments have demonstrated that this type of attack occurred in the immediate vicinity of a catalyst particle, which for the most part remained static on the graphite surface during the process. Once formed, the pits were observed to expand and in some cases become perceptibly deeper if the temperature was held at about 100°C. It was also apparent that the edges of the pit appeared to be decorated with a very thin layer of copper oxide that could have been intimately involved in both the creation and subsequent expansion processes.

This sequence of events is consistent with the notion that dissociation of hydrogen is taking place on the catalyst particle surface and the atomic species generated in this process are free to migrate onto the adjacent areas of the graphite support via a "spillover" mechanism. These species are known to be extremely reactive toward the π-electrons present on the graphite basal planes and such action has been shown to lead to the creation of pits in these surface regions (44). The expansion of these features can be rationalized according to the argument that the adherent layer of copper oxide provides a continued source of atomic hydrogen at these locations, which are remote from that of the initial particle that remains within the pit. It was significant to find that this form of attack did not occur when diamond was used as the support medium, a material where the basal planes do not possess a delocalized cloud of π-electrons.

A similar form of pitting attack of the basal plane by atomic hydrogen has also been found to occur when other additives have been dispersed on graphite. Using a combination of CAEM and *in situ* electron diffraction techniques, Rodriguez and Baker (45) reported that this action occurred when either MoS_2–graphite or FeS_2–graphite specimens were exposed to hydrogen at room temperature and became more intense at 100°C. Continued heating to temperatures in excess of 500°C resulted in a termination of pitting, conditions that appeared to coincide with a conversion of the additive to the metallic state. This pattern of behavior is consistent with the current observations, which showed that the pitting action ceased when the oxide had been reduced to copper.

The removal of carbon via the interaction with atomic hydrogen to form gaseous hydrocarbons is known to take place at moderate temperatures and while the process proceeds in an indiscriminate fashion on amorphous carbon, attack tends to take place preferentially on the basal plane regions of graphite (46–49). In both cases, the results of this action would be expected to be manifested by an increase in the surface area of the respective support medium, which was indeed found from the experimental data. Since the attack of the graphite surface occurred simultaneously with the reduction of CuO to Cu_2O, it is suggested that the latter oxide might be the active species responsible for the dissociation of the molecular hydrogen. Under such circumstances one would predict that the stability of cuprous state would have a direct impact on the degree of severity of the catalyzed gasification reaction and, as a consequence, the increase in the surface area of the carbon support material. In this context it is interesting to find that an activated carbon supported copper oxide system was found to be most resistant to reduction . This feature was attributed to the presence of a large concentration of oxygen groups on the activated carbon surface that served to stabilize the formation of Cu_2O (50). The high surface area activated carbon used in the present study also possesses a significant concentration of surface oxygen groups that would be expected to stabilize Cu_2O to a certain degree even in a hydrogen environment (51). As a consequence, the Cu_2O-catalyzed dissociation of hydrogen will be favored and the ramifications of this process displayed by an increase in the surface area of the sample.

SUMMARY

The results of this study have clearly demonstrated that the nature of the carbonaceous support medium can exert a significant impact on not only the morphological characteristics, but also the chemical state of copper particles at various stages of a reduction step. Controlled atmosphere electron microscopy studies combined with *in situ* electron diffraction analysis and other techniques have demonstrated that the ease of reduction of CuO is dependent upon the nature of the carbon material and surface properties. From these experiments it is tentatively concluded that Cu^0 sites at the surface of Cu_2O particles can dissociate molecular hydrogen and that these atomic species, which have the ability to remove atoms from amorphous and graphitic forms of carbon, are responsible for producing extensive modifications the surface structure of these support media. In contrast, Cu_2O does not exhibit the same degree of stability on a diamond support, and furthermore, dissociated hydrogen species do not appear to interact with this allotrope of carbon at temperatures below 600°C.

ACKNOWLEDGMENTS

Support for this work was provided by the National Science Foundation under Grant CTS-9415335.

REFERENCES

1. Thomas, C. L., "Catalytic Processes and Proven Catalysts," Academic Press, New York, 1970.
2. Bridger, G. W., and Spencer, M. S., "Catalysis Handbook" (M. V. Twigg, Ed.), 2nd ed., Wolfe, U.K., 1992.
3. Carley, A. F., Rajuman, M. K., and Roberts, M. W., *J. Solid State Chem.* **106**, 156 (1993).
4. Jirka, I., *Surf. Sci.* **232**, 307 (1990).
5. Nardo, S. D., Lozzi, L., Passacantando, M., Picozzi, P., Santucci, S., and De Crescenzi, M., *Surf. Sci.* **287**, 1087 (1993).
6. Nardo, S. D., Lozzi, L., Passacantando, M., Picozzi, P., Santucci, S., and De Crescenzi, M., *Surf. Sci.* **307**, 922 (1994).

7. Dandekar, A., Ph.D. thesis, Pennsylvania State University, 1998.
8. Rao, R., Ph.D. thesis, Pennsylvania State University, in progress.
9. Jernigan, G. G., and Somorjai, G. A., *J. Catal.* **147**, 567 (1994).
10. Field, J. E., "Properties of Diamond," Academic Press, London, 1979.
11. Bundy, F. P., Strong, H. M., and Wentorf, R. H., *in* "Chemistry and Physics of Carbon" (P. L. Walker, Jr., and P. A. Thrower, Eds.), Vol. 10, p. 213. Dekker, New York, 1973.
12. Marsh, J. B., and Farnsworth, H. E., *Surf. Sci.* **1**, 3 (1964).
13. Messier, R., Spear, K. E., Badzian, T., Badzian, A. R., Bachmann, P., and Roy, R., *Thin Solid Films* **153**, 1 (1987).
14. Pate, B. B., *Surf. Sci.* **165**, 83 (1986).
15. Hamza, A. V., Kubiak, G. D., and Stulen, R. H., *Surf. Sci.* **237**, 35 (1990).
16. Zheng, X. M., and Smith, P. V., *Surf. Sci.* **261**, 394 (1992).
17. Harrison, J. A., White, C. T., Cotton, R. J., and Brenner, D. W., *Surf. Sci.* **271**, 57 (1992).
18. Cinti, R. C., Mathis, B. S., and Bonnot, A. M., *Surf. Sci.* **279**, 265 (1992).
19. Lurie, P. G., and Wilson, J. M., *Surf. Sci.* **65**, 453 (1977).
20. Matsumoto, S., and Setaka, N., *Carbon* **17**, 485 (1979).
21. Thomas, R. E., Rudder, R. A., and Markunas, R. J., *J. Vac. Sci. Technol. A* **10**, 2451 (1992).
22. Pepper, S. V., *Surf. Sci.* **123**, 47 (1982).
23. Baker, R. T. K., and Chludzinski, J. J., *Carbon* **19**, 75 (1981).
24. Derouane, E. G., Chludzinski, J. J., and Baker, R. T. K., *J. Catal.* **85**, 187 (1984).
25. Scholten, J. J. F., and Konvalinka, J. A., *Trans. Faraday Soc.* **65**, 2465 (1969).
26. Pilliar, R. M., and Nutting, J., *Phil. Mag.* **6**, 181 (1967).
27. Rao, R., Dandekar, A., Baker, R. T. K., and Vannice, M. A., *J. Catal.* **171**, 406 (1997).
28. Singoredjo, L., Slagt, M., van Wees, J., Kapteijn, F., and Moulijn, J. A., *Catal. Today* **7**, 157 (1990).
29. Nozaki, F., Yamazaki, K., and Inomata, T., *Chem. Lett.* 512 (1977).
30. Imai, J., Suzuki, T., and Kaneko, K., *Catal. Lett.* **20**, 133 (1993).
31. Yamashita, H., Yamada, H., and Tomita, A., *Appl. Catal.* **78**, L1 (1991).
32. Rodriguez, N. M., Oh, S. G., Downs, W. B., Pattabiraman, P., and Baker, R. T. K., *Rev. Sci. Instrum.* **61**, 1863 (1990).
33. Crystallographic Data, JCPDS file.
34. Hurst, N. W., Gentry, S. J., Jones, A., and McNicol, B. D., *Catal. Rev.-Sci. Eng.* **24**, 233 (1982).
35. Boyce, A. L., Graville, S. R., Sermon, P. A., and Vong, M. S. W., *React. Kinet. Catal. Lett.* **44**, 1 (1991).
36. Baker, R. T. K., *J. Adhesion* **52**, 13 (1995).
37. Nakayama, T., Arai, M., and Nishiyama, Y., *J. Catal.* **79**, 497 (1983).
38. Ruckenstein, E., and Lee, S. H., *J. Catal.* **86**, 457 (1984).
39. Sushumna, I., and Ruckenstein, E., *J. Catal.* **94**, 239 (1985).
40. Chen, A. A., Vannice, M. A., and Phillips, J., *J. Catal.* **116**, 568 (1989).
41. Handy, B. E., Dumesic, J. A., Sherwood, R. D., and Baker, R. T. K., *J. Catal.* **124**, 160 (1990).
42. Ruckenstein, E., *in* "Metal-Support Interactions in Catalysis, Sintering and Redispersion" (S. A. Stevenson *et al.*, Eds.), p. 230. Van Nostrand-Reinhold, New York, 1987.
43. Allard, L. F., Voelkl, E., and Datye, A. K., *J. Mater. Sci.* **29**, 5612 (1994).
44. Chen, J. P., and Yang, R. T., *Surf. Sci.* **216**, 481 (1989).
45. Rodriguez, N. M., and Baker, R. T. K., *J. Catal.* **140**, 287 (1993).
46. Vastola, F. J., Walker, P. L., Jr., and Wightman, J. P., *Carbon* **1**, 11 (1963).
47. Gill, P. S., Toomey, R. E., and Moser, H. C., *Carbon* **5**, 43 (1967).
48. Wood, B. J., and Wise, H., *J. Phys. Chem.* **73**, 1348 (1969).
49. McCarroll, B., and McKee, D. W., *Carbon* **9**, 301 (1971).
50. Jirka, I., and Dubsky, J., *Appl. Surf. Sci.* **40**, 135 (1989).
51. Dandekar, A., Baker, R. T. K., and Vannice, M. A., *Carbon* **36**, 1821 (1998).